ISSN 1674-1056
http://cpb.iphy.ac.cn
http://iopscience.iop.org/cpb
中国物理 B
Chinese Physics
中国物理
Chinese Physics B

First principles study of stability, mechanical and electronic properties of chromium silicides

Bo Ren(任博), De-Hong Lu(卢德宏), Rong Zhou(周荣), De-Peng Ji(姬德朋), Ming-Yu Hu(胡明钰), Jing Feng(冯晶)
Citation: Chin. Phys. B . 2018, 27(10): 107102. **doi:** 10.1088/1674-1056/27/10/107102

Journal homepage: http://cpb.iphy.ac.cn; http://iopscience.iop.org/cpb

What follows is a list of articles you may be interested in

Dirac states from $p_{x,y}$ orbitals in the buckled honeycomb structures: A tight-binding model and first-principles combined study

Shi-Ru Song(宋士儒), Ji-Hui Yang(杨吉辉), Shi-Xuan Du(杜世萱), Hong-Jun Gao(高鸿钧), Boris I Yakobson
Chin. Phys. B . 2018, 27(8): 087101. **doi:** 10.1088/1674-1056/27/8/087101

The structural, electronic, and optical properties of organic-inorganic mixed halide perovskites $CH_3NH_3Pb(I_{1-y}X_y)_3$ (X=Cl, Br)

Miao Jiang(姜淼), Naihang Deng(邓乃航), Li Wang(王丽), Haiming Xie(谢海明), Yongqing Qiu(仇永清)
Chin. Phys. B . 2018, 27(6): 067102. **doi:** 10.1088/1674-1056/27/6/067102

Effect of pressure on the elastic properties and optoelectronic behavior of $Zn_4B_6O_{13}$: First-principles investigation

Pei-Da Wang(王培达), Zhen-Yuan Jia(贾镇源), Yu-Han Zhong(钟玉菡), Hua-Yue Mei(梅华悦), Chun-Mei Li(李春梅), Nan-Pu Cheng(程南璞)
Chin. Phys. B . 2018, 27(5): 057101. **doi:** 10.1088/1674-1056/27/5/057101

Magnetism, optical, and thermoelectric response of $CdFe_2O_4$ by using DFT scheme

Q Mahmood, M Yaseen, K C Bhamu, Asif Mahmood, Y Javed, Shahid M Ramay
Chin. Phys. B . 2018, 27(3): 037103. **doi:** 10.1088/1674-1056/27/3/037103

Structural, electronic, and mechanical properties of cubic TiO_2: A first-principles study

Debashish Dash, Chandan K Pandey, Saurabh Chaudhury, Susanta K Tripathy
Chin. Phys. B . 2018, 27(1): 017102. **doi:** 10.1088/1674-1056/27/1/017102

First principles study of stability, mechanical, and electronic properties of chromium silicides*

Bo Ren(任博), De-Hong Lu(卢德宏)†, Rong Zhou(周荣),
De-Peng Ji(姬德朋), Ming-Yu Hu(胡明钰), and Jing Feng(冯晶)

Faculty of Materials Science and Engineering, Kunming University of Science and Technology, Kunming 650093, *China*

(Received 17 May 2018; revised manuscript received 3 July 2018; published online 10 September 2018)

Through the first principles calculations, the chemical stability, mechanical, and electronic properties of chromium silicides are predicted. Estimating enthalpies and binding energies, density state density and electron density distribution are combined to analyse the thermodynamic stability and physical properties of chrome-silicon binary compounds. The chromium silicide includes Cr_3Si, Cr_5Si_3, CrSi, and $CrSi_2$. The chemical stability and the information about electronic structure, mechanical properties, Debye temperature, and anisotropy properties are obtained by density functional theory and Debye quasi-harmonic approximation. Meanwhile, the calculation of elastic modulus shows that Cr_3Si has the highest body modulus value (251 GPa) and $CrSi_2$ possesses the highest shear modulus (169.5 GPa) and Young's modulus (394.9 GPa). In addition, the Debye temperature and the speed of sound of these Cr–Si compounds are also calculated. Since the calculated bulk modulus is different from Young's modulus anisotropy index, and also different from Young's modulus of a three-dimensional surface shape, the different mechanical anisotropies of all the compounds are obtained.

Keywords: density functional theory, electronic structures, mechanical properties, anisotropy

PACS: 71.15.Mb, 71.23.–K, 62.20.–x, 75.30.Gw **DOI:** 10.1088/1674-1056/27/10/107102

1. Introduction

Transition metal silicides possess the characteristics of a high melting point, outstanding resistance to high temperature oxidation, high creep strength, excellent mechanical properties, and chemical stability. Therefore, they can be used in high-temperature structures.[1–3]

Researchers have shown great interest in transition metal silicides such as Cr–Si alloy compounds including Cr_3Si, Cr_5Si_3, CrSi, and $CrSi_2$. Yeh *et al.* fabricated a chrome-silicon alloy for coating the metal surface by self-propagating high-temperature synthesis.[4] Wang *et al.* prepared a chrome-silicon alloy using a water-cooled copper mold laser furnace, investigated microstructure characteristics, and discussed the formation mechanism of the phases in the Cr–Si alloy.[5,6] Kong *et al.* revealed the crystal structures of Cr–Si compounds by combining experimental measurements and density functional theory calculation. Schuster *et al.*[7,8] proposed a new thermodynamic description of the Cr–Si binary system. Krijn *et al.*[9] calculated the electronic structure and optical properties of Cr_2Si according to the first principles, which are basically consistent with the experimental results. However, the mechanical properties, electronic properties and elastic anisotropy of Cr–Si compounds have not been studied systematically, owing to the difficulty in performing their syntheses and characterizations.

In this paper, the stability, chemical bonding properties, mechanical properties, and Debye temperature of chromium-silicon compounds are systematically studied by using the first-principles calculation. The work will be helpful in choosing reinforcing phases in the materials for aerospace industry or high temperature wear resistant materials.

2. Calculation methods

All of the theoretical calculations in this paper were based on density functional theory (DFT) in the Cambridge Sequential Almighty Package (CASTEP) program.[10,11] For setting up crystal structure models of the Cr–Si compounds correctly, optimization of the models was carried out by using the planar wave expansion method, and the interaction between the atom core and valence electrons was achieved by using the ultra-soft pseudo-potential. For Cr and Si atoms, the electronic states Cr: $3s^2 3p^6 3d^5 4s^1$ and Si: $3s^2 3p^2$ were treated as valence states. Perdew *et al.* calculated the compound variation and related functions by a generalized gradient approximation.[12]

As shown in Fig. 1,[13] the Cr_xSi_y binary compounds contain four phases and three different types of lattice, i.e., the square lattice (Cr_5Si_3), cubic (CrSi, Cr_3Si), and hexagonal ($CrSi_2$) crystal. The melting point of Cr_3Si is highest (1770 °C) and that of CrSi is lowest (1413 °C). The crystal structures of the Cr_xSi_y system are shown in Fig. 2. Energy integration in the first irreducible Brillouin zone was characterized with the *k*-point method proposed by Monkhorst and Pack,[14] and the *k* point mesh was selected as $10\times10\times10$ for all structures. The planar wave expansion in reciprocal space

*Project supported by the National Natural Science Foundation of China (Grant No. 51265019).
†Corresponding author. E-mail: ldhongkust@126.com
© 2018 Chinese Physical Society and IOP Publishing Ltd

was conducted by using a maximum energy cutoff of 450 eV. The crystal structure optimization was performed based on the Broydene–Fletchere–Goldarbe–Shanno (BFGS) method, which minimizes the total energy whose variation during the process of optimization is about 2×10^{-6} eV and the force on different atoms converges to 0.05 eV/Å.

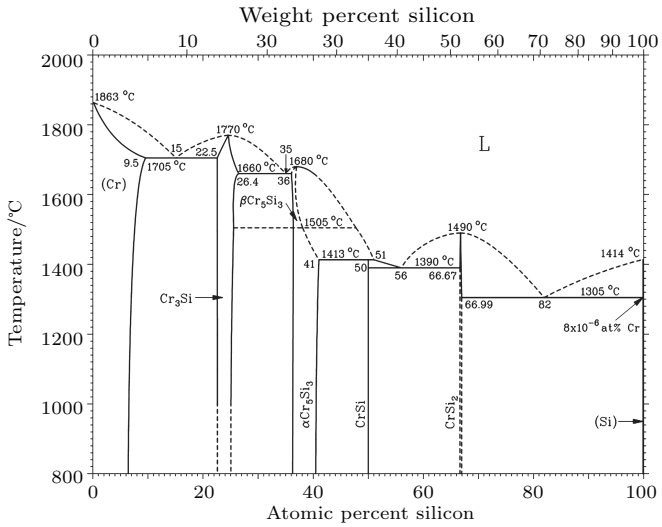


Fig. 1. Cr–Si equilibrium phase diagram.[13]

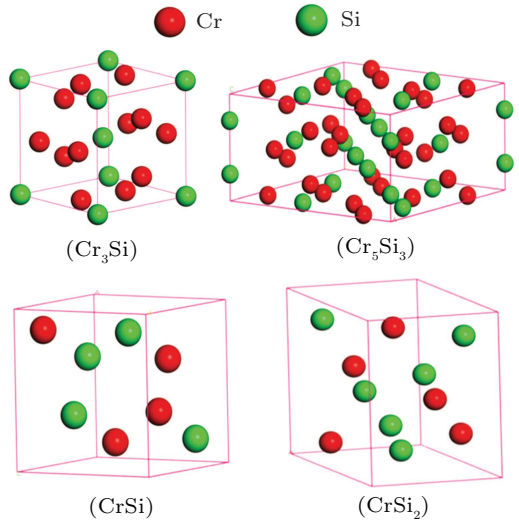


Fig. 2. (color online) Crystal structures of the Cr–Si compounds.

3. Results and discussion

3.1. Stability

In order to study the thermodynamic stability of Cr–Si binary compounds, their enthalpies of formation and cohesion are calculated and the two energy formulas are defined as follows:

$$E_{\mathrm{coh}}(\mathrm{Cr}_x\mathrm{Si}_y) = \frac{E_{\mathrm{tot}}(\mathrm{Cr}_x\mathrm{Si}_y) - xE_{\mathrm{iso}}(\mathrm{Cr}) - yE_{\mathrm{iso}}(\mathrm{Si})}{x+y}, \quad (1)$$

$$\Delta H_{\mathrm{r}}(\mathrm{Cr}_x\mathrm{Si}_y) = \frac{E_{\mathrm{tot}}(\mathrm{Cr}_x\mathrm{Si}_y) - xE_{\mathrm{bin}}(\mathrm{Cr}) - yE_{\mathrm{bin}}(\mathrm{Si})}{x+y}, \quad (2)$$

where $E_{\mathrm{coh}}(\mathrm{Cr}_x\mathrm{Si}_y)$ and $\triangle H_{\mathrm{r}}(\mathrm{Cr}_x\mathrm{Si}_y)$ represent the cohesive energy and formation enthalpy of the chrome-silicon compound, respectively; $E_{\mathrm{tot}}(\mathrm{Cr}_x\mathrm{Si}_y)$, $E_{\mathrm{iso}}(\mathrm{Cr})$, and $E_{\mathrm{iso}}(\mathrm{C})$ denote the total energy of the $\mathrm{Cr}_x\mathrm{Si}_y$ phase, a single Cr atom and a single Si atom, respectively; E_{bin} (Cr) and E_{bin} (Si) refer to the cohesive energy of Cr atom and Si atom, respectively.[15,16]

Table 1. Calculated parameters (a, b, c in unit Å), cohesive energy (eV/atom), and formation enthalpy (eV/atom) of Cr–Si compounds.

Species	Space group	a/Å	b/Å	c/Å	Cohesive energy/(eV/atom)	Formation enthalpy/(eV/atom)
Cr	*Im*3*m*	2.850	2.850	2.850	10.207	
		2.885[d]	2.885[d]	2.885[d]		
Cr_3Si	*PM*-3*N*	4.513	4.513	4.513	9.368	0.355
		4.568[a]	4.568[a]	4.568[a]		–0.357[d]
		4.556[e]	4.556[e]	4.556[e]		–0.327[j]
		4.555[h]	4.555[h]	4.555[h]		
Cr_5Si_3	*I*4/*MCM*	9.069	9.069	4.587	8.727	–0.314
		9.170[a]	9.170[a]	4.636[a]		–0.348[g]
						–0.337[i]
						–0.338j
CrSi	*P*213	4.592	4.592	4.592	–8.126	–0.302
		4.620[a]	4.620[a]	4.620[a]		–0.286[c]
						–0.309[d]
						–0.315[i]
						–0.313[j]
$CrSi_2$	*P*6222	4.397	4.397	6.369	7.406	–0.284
		4.428[a]	4.428[a]	6.368[a]		–0.276[d]
		4.428[b]	4.428[b]	6.369[b]		–0.283[i]
		4.425[f]	4.425[f]	6.373[f]		–0.270[j]
Si	*FD*-3*M*	5.465	5.465	5.465	5.429	
		5.431[d]	5.431[d]	5.431[d]		

[a]Cal. in Ref. [17], [b]Cal. in Ref. [18], [c]Cal. in Ref. [19], [d]Cal. in Ref. [13], [e]Cal. in Ref. [20], [f]Cal. in Ref. [21], [g]Cal. in Ref. [22], [h]Cal. in Ref. [23], [i]Cal. in Ref. [7], [j]Cal. in Ref. [24].

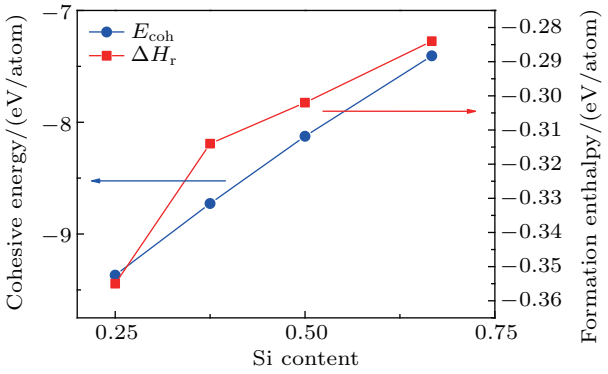


Fig. 3. (color online) Plots of calculated cohesive energy and formation energy versus Si content of Cr–Si compounds.

Table 1 shows the calculated parameters about thermodynamic stability, such as cell parameters, cohesive energy, and formation enthalpy, and their comparison with other researchers' results. It can be seen that the crystal parameters of the Cr–Si system match well with other experimental and calculated values.[7,13,16–24] Furthermore, the tiny deviation among them can be attributed to the different calculation methods and experimental conditions. According to Table 1, the cohesive energies of the Cr–Si compounds decrease from −10.207 eV/atom to −7.406 eV/atom, but the Si content in the crystal cell increases from 0.25 to 0.67, which correspond to those of Cr_3Si, Cr_5Si_3, CrSi, and $CrSi_2$ as shown in Fig. 3. In the meantime, the formation enthalpy varies with the Si content increasing similarly.[25] The lowest formation enthalpy is −0.355 eV/atom for Cr_3Si, while the highest one is −0.284 eV/atom for $CrSi_2$. All values of cohesive energy and formation enthalpy are negative, which means that the thermodynamic properties of all Cr–Si compounds are stable.

According to the order of the formation enthalpy and the bonding energy of the Cr–Si compounds, the order of thermal stability of Cr–Si compounds is Cr_3Si>Cr_5Si_3>CrSi>$CrSi_2$. Therefore, Cr_3Si is the most stable in thermal properties among CrSi binary compounds.

3.2. Electronic structures

In order to analyze the chemical bond properties of chrome-silicon compounds and the electron density distribution of the electronic structure, the total state of atoms (TDOS) and the partial state of charge (PDOS) are shown in Fig. 4.

The nature of the magnetic characteristic can be understood from the spin-polarized total density of states. Generally speaking, the up and down states are symmetric, but the up and down states of CrSi are dissymmetric, which indicates the magnetic characteristic.[26,27] Actually, the low and high valence bands are almost symmetric, and the up and down states are dissymmetric with respect to the Fermi level but very close to the Fermi level. Comparing with other compounds, we can guess they have no magnetic characteristics, because the down and up states are symmetric.

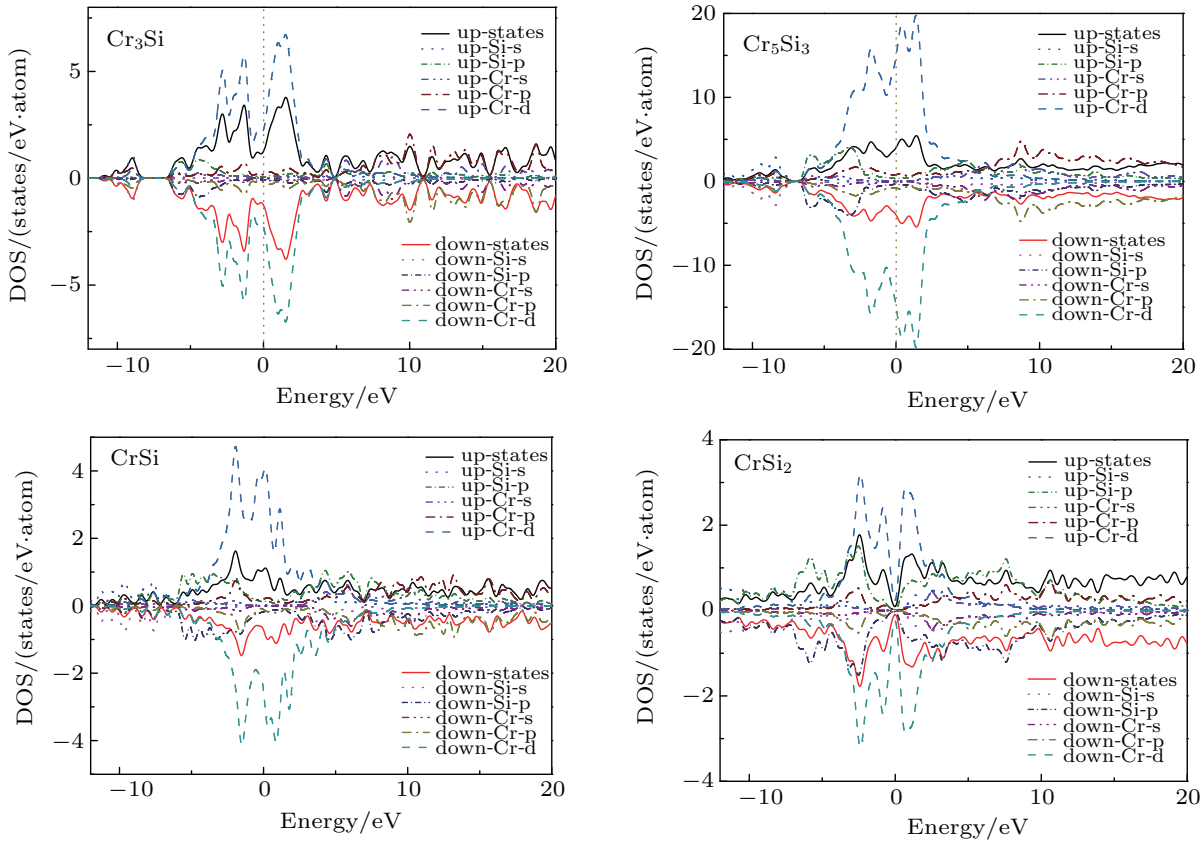


Fig. 4. (color online) Plots of calculated total density of states (TDOS) and partial density of states (PDOS)versus energy for the Fe and Cr–Si system. Dashed line represents the Fermi level.

The electron density values are greatly larger than zero even in the interstitial regions, which presents the strong metallic characteristic of Cr–Si compounds.[28,29] For all chromium silicides, the d band of Cr dominates the total state density, because the variation of d bond corresponds most to the total state density. Their Fermi level lies at the shoulder of the TDOS peak, which means that they are all stable. It is consistent with the results of binding energies and formation enthalpy.

Mulliken population analysis is one parameter to reveal the material interior chemical bonding characteristics. The average bonding length and average population can be calculated from the following equations:[30]

$$\bar{L}(AB) = \frac{\sum_i L_i N_i}{\sum_i N_i}, \tag{3}$$

$$\bar{n}(AB) = \frac{\sum_i n_i N_i}{\sum_i N_i}. \tag{4}$$

Here $\bar{L}(AB)$ is the average bond length and $\bar{n}(AB)$ is the mean bond population. The N_i and L_i represent the total number of i bonds in the cell and the bond length of i type, respectively. The population analysis results are listed in Table 2. For all of the Cr–Si compounds, Si carries the positive charges and the values vary from 0.19e to 0.42e. The Cr_5Si_3 shows the stronger ionicity due to the fact that the largest negative charges are carried by Cr atoms of it. In the Cr–Si compounds, there are three kinds of Si–Cr, Cr–Cr, and Si–Si bonds. All compounds have Si–Cr bonds, which have positive values for the average population. The average population of Si–Cr bonds is larger in each of Cr_3Si and CrSi, implying the Si–Cr bond is strong. In the case of $CrSi_2$, both the Si–Cr and Si–Si bonds have positive values for the overlap population, indicating a covalent bonding character. In addition, the Cr–Cr bond has a negative overlap population in the Cr–Si compound, which implies that there exists an anti-bonding effect in the chromium-silicon compound.

Table 2. Population analysis results of the studied Cr–Si compounds: Total refers to electron occupation; Charge denotes electron transition; $\bar{L}(AB)$ represents average bonding length (in unit Å); and $\bar{n}(AB)$ means the average population (electrons/bond).

Species	Atom	s	p	d	Total	Charge(e)	Bond	$\bar{L}(AB)$	$\bar{n}(AB)$
Cr_3Si	Si	1.11	2.61	0.00	3.73	0.27	Si–Cr	2.523	0.440
	Cr	2.23	6.74	5.12	14.09	-0.09	Cr–Cr	2.663	–0.382
Cr_5Si_3	Si1	1.18	2.63	0.00	3.81	0.19	Si–Cr	2.461	0.265
	Si_2	1.13	2.51	0.00	3.64	0.36	Cr–Cr	2.718	–0.171
	Cr1	2.25	6.81	5.14	14.20	–0.20	Si–Si	2.294	0.98
	Cr2	2.25	6.73	5.20	14.18	–0.18			
CrSi	Si	1.15	2.43	0.00	3.58	0.42	Si–Cr	2.397	0.405
	Cr	2.35	6.81	5.26	14.42	–0.42	Cr–Cr	2.816	–1.28
							Si–Si	2.834	0.02
$CrSi_2$	Si	1.22	2.48	0.00	3.70	0.30	Si–Cr	2.495	0.323
	Cr	2.30	6.79	5.51	14.60	–0.60	Si–Si	2.491	0.183

From Fig. 4, it can be seen that although the Cr-d orbit plays a major role in TDOS from −4 eV to 4 eV, the Cr-p orbit plays a major role in a range from 8 eV to 16 eV. The p band of Si located near the Fermi level overlaps with the orbit of Cr to some extent, which implies a covalent interaction between Si and Cr atoms p–d orbital hybridization. Therefore, strong covalent bonding exists among these compounds, which is advantageous for improving their high-temperature creep strength, shear strength, and hardness. The valence band of the orbit and the valence band of the top of the orbit are mainly composed of the p orbit and the d orbit of the Cr atom, but the contribution of the s and p orbits of the Cr atom cannot be ignored. The s orbit clearly illustrates that the evolutions of the silicon content forbidden bands of metal-rich compounds are formed in the Si-s orbit from −8 eV to −7 eV, whereas in disilicides from −12 eV to −4 eV, Si-s band with p bands shows the continuity of the TDOS. In addition, the s orbit and p orbit of Si contribute significantly to TDOS in the conduction band for Cr_5Si_3, indicating that its conductivity is higher than that of other Cr_xSi_y compounds.

Figure 5 shows the electron density distributions in Cr–Al binary compounds. As can be seen from Figs. 5(a), 5(c), 5(e), and 5(g), all Cr and Si atoms in the core region have smaller gap regions and larger values in color bar. In these figures, the Cr and Si atoms show the covalent bond and elongated outline along the Si–Si bond axis, indicating that they have covalent interactions. From Cr_3Si to $CrSi_2$, there are covalent bonds between Si atoms. We can also find more detailed information about the chemical bond properties from the different distributions of electron density in Figs. 5(b), 5(d), 5(f), and 5(h). Some non-localized electrons pass through the circular profile of the region between Cr and Si atoms, which means that they have covalent and metallic bonds. The blue areas surrounding the Cr and Si atoms suggest the existence of covalent bonds. Chromium

silicon compounds possess covalent bonds and metal bonds, which makes the metal silicide atoms have good plasticity and high atomic binding. In addition, we also find the anti-bonding effects of chromium-silicon compounds, that is, chromium-chromium bonding. Based on the above discussion, we conclude that the combination of these silicides is a combination of covalent and metal bonds, resulting in a high melting point, high hardness, and high temperature oxidation resistance.

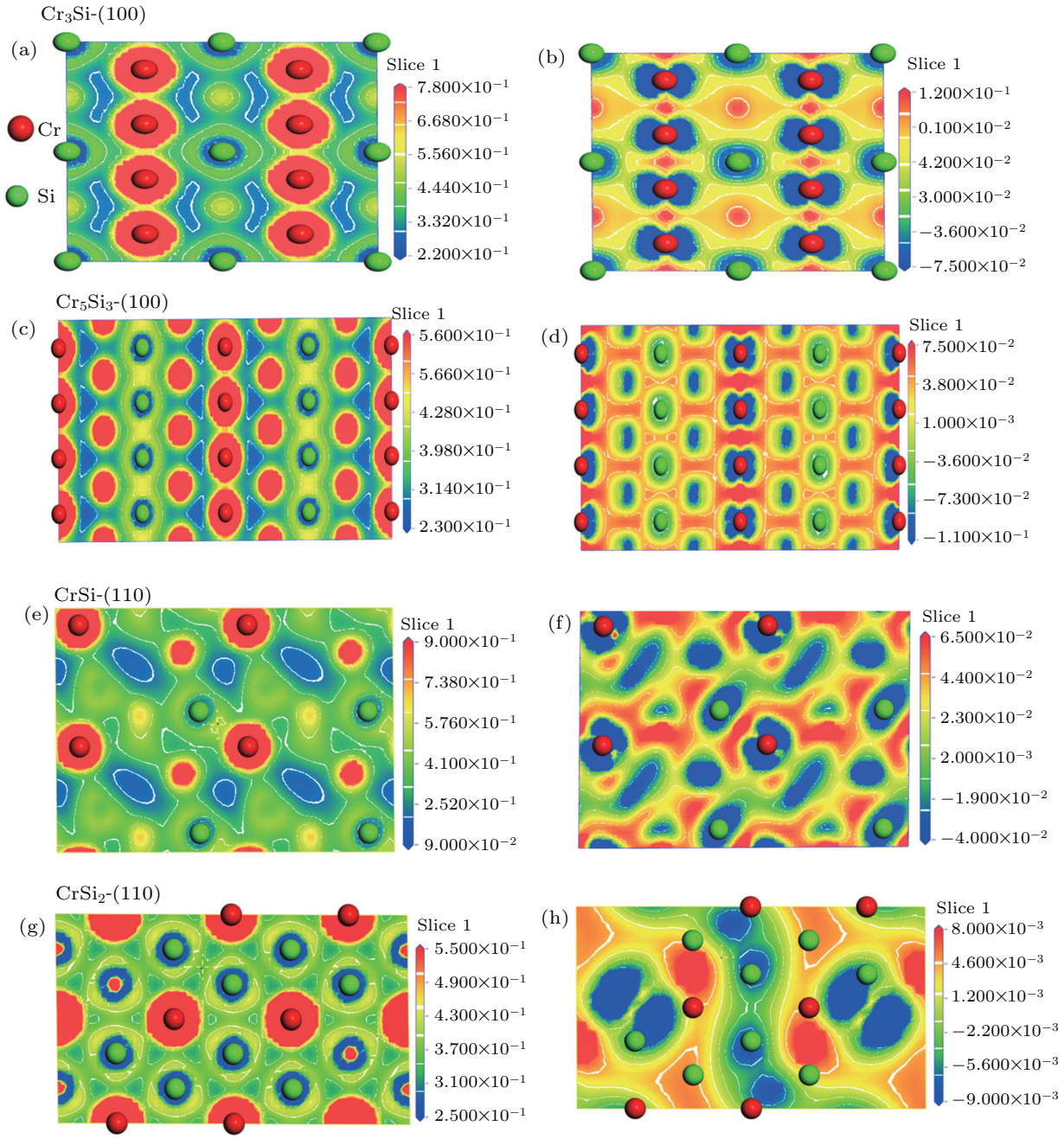


Fig. 5. (color online) ((a),(c), (e), (g)) Total electron density distribution contours and ((b), (d), (f), (h)) electron density difference distribution contours for Cr–Si compounds.

3.3. Mechanical stability and elastic properties

Based on the generalized Hook law, the elastic constants of Cr–Si compounds are calculated by using the stress-strain method. The structure of the crystal is calculated by several different strain modes, and the corresponding Cauchy stress tensor is evaluated.

According to these strain–stress relationships in Eq. (5),[31] the related elastic constants are determined.

$$\begin{pmatrix} \sigma_1 \\ \sigma_2 \\ \sigma_3 \\ \tau_4 \\ \tau_5 \\ \tau_6 \end{pmatrix} = \begin{pmatrix} C_{11} & C_{12} & C_{13} & C_{14} & C_{15} & C_{16} \\ & C_{22} & C_{23} & C_{24} & C_{25} & C_{26} \\ & & C_{33} & C_{34} & C_{35} & C_{36} \\ & & & C_{44} & C_{45} & C_{46} \\ & & & & C_{55} & C_{56} \\ & & & & & C_{66} \end{pmatrix} \begin{pmatrix} \varepsilon_1 \\ \varepsilon_2 \\ \varepsilon_3 \\ \gamma_4 \\ \gamma_5 \\ \gamma_6 \end{pmatrix}. \quad (5)$$

The symmetry of crystal has a dominant role in affecting the total number of independent elastic constants. In the equation, C_{ij} represents the elastic constant, σ_i the normal stress, τ_i the shear stress, ε_i the shearing strain, and γ_i the corresponding normal. When the system is highly symmetric, the required C_{ij} calculations can greatly reduce the different strain modes.

The calculated elastic constants of the Cr–Si system are summarized in Table 2. The stabilities of these compounds are studied from the mechanical properties.[32] Based on Born-Huang's lattice dynamics theory, the strain energy of the mechanical stability of a structure must be positive in one of the conditions for any uniform elastic deformation as indicated below.[30,33,34]

For cubic system (for Cr_3Si, CrSi):

$$(C_{11}C_{12}) > 0, \quad C_{11} > 0, \quad C_{44} > 0, \quad C_{11} + 2C_{12} >; \tag{6}$$

for tetragonal system (for Cr_5Si_3):

$$\begin{aligned} &C_{11} > C_{12} >, \quad 2C_{13}^2 < C_{33}(C_{11} + C_{12}), \\ &C_{44} > 0, \quad 2C_{16}^2 < C_{66}(C_{11}C_{12}); \end{aligned} \tag{7}$$

for hexagonal system (for $CrSi_2$):

$$C_{11} > 0,\ C_{44} > 0,\ C_{11} - C_{22} > 0,\ (C_{11} + C_{12})C_{33} > 2C_{13}^2. \tag{8}$$

Table 3. Calculated elastic constants (in unit GPa) of Cr–Si compounds.

Species	C_{ij}								
	C_{11}	C_{12}	C_{13}	C_{22}	C_{23}	C_{33}	C_{44}	C_{55}	C_{66}
Cr	417.6	147.5	147.5	417.6	147.5	417.6	97.3	97.3	97.3
	350[a]	67.8[a]					129[a]		
Cr_3Si	480.8	136.1	136.1	480.8	136.1	480.8	149.4	149.4	149.4
	416.0[a]	98.7[a]					129[a]		
Cr_5Si_3	431.2	140.8	112.8	431.2	112.8	404.5	117.4	117.4	152.2
CrSi	390.5	112.3	112.3	390.5	112.3	390.5	125.7	125.7	125.7
$CrSi_2$	418.1	51.6	105.2	418.1	105.2	408.2	170.2	170.2	183.2
	372.2[b]	45.3[b]	82.6[b]			385.2[b]	149.1[b]		
	454.0[c]	72.6[c]	118.5[c]			453.0[c]	172.7[c]		
	350.9[d]	107.2[d]	92.97[d]			471.7[d]	201.9[d]		171.0[d]
Si	157.5	39.7	39.7	157.5	39.7	157.5	98.8	98.8	98.8
	166.3[b]	65.1[b]					79.4[b]		

[a]Cal. in Ref. [35], [b]Cal. in Ref. [36], [c]Cal. in Ref. [37], [d]Cal. in Ref. [38].

From Table 3, we find that the calculated elastic constant values are consistent with the above criteria, indicating that all Cr–Si compounds are elastically stable. Moreover, Table 3 shows the comparisons among the results obtained in this paper, the results obtained by other methods, and the experimental results. In Cr–Si binary compounds, the Cr_3Si obtained C_{11}, C_{22}, and C_{33} (the same value 480.8 GPa) are larger elastic constants than other compounds', showing that they are very incompressible under uniaxial stress along the x (ε_{11}), y (ε_{22}), or (ε_{33}) axis. The C_{44}, C_{55}, and C_{66} represent the shear moduli on the (100), (010), and (001) crystal plane, respectively. In Table 2, the values for $CrSi_2$ have the largest C_{44}, C_{55}, and C_{66} value of 170.2 GPa, 170.2 GPa, and 183.2 GPa, respectively.

Table 4. Calculated bulk moduli, shear moduli, Young's moduli, and Poisson's ratios of CrSi compounds.

Species	B_V	B_R	B_{VRH}	G_V	G_R	G_{VRH}	E	γ	B/G
Cr	255.5	255.5	255.5	123.2	115.8	119.5	310.1	0.298	2.14
							328[b]		
Cr_3Si	251.0	251.0	251.0	158.6	157.8	158.1	392.0	0.239	1.59
							378[b]		
Cr_5Si_3	222.2	221.5	221.9	137.5	135.3	136.4	339.6	0.244	1.63
CrSi	205.0	205.0	205.0	131.1	130.7	130.9	323.8	0.237	1.56
						107.7[a]	260.9[a]		
$CrSi_2$	196.5	196.0	196.3	170.2	168.8	169.5	394.9	0.164	1.16
			193.1 c			173.6[c]	433.9[c]		1.53[c]
			219.9[d]			177.3[d]	419.3[d]	0.18[d]	1.24[d]
			219.7[d]			176.4[d]	417.5[d]	0.18[d]	1.25[d]
			219.8[d]			176.9[d]	418.4[d]	0.18[d]	1.24[d]
			172.3[e]			153.6[e]	355.2[e]	0.16[e]	1.12[e]
Si	78.9	78.9	78.9	82.8	77.7	80.3	179.9	0.120	0.983

[a]Cal. in Ref. [40], [b]Cal. in Ref. [35], [c]Cal. in Ref. [38], [d]Cal. in Ref. [37], [e]Cal. in Ref. [36].

The bulk modulus (B), shear modulus (G), Young's modulus (E), and Poisson's ratio (σ) are calculated using Eqs. (9)–(12), and the polycrystalline crystals are estimated with independent single crystal elastic constants according to the Voigt–Reuss–Hill (VGH) approximation.[39]

$$B_{\mathrm{VRH}} = \frac{1}{2}\left(B_{\mathrm{V}} + B_{\mathrm{R}}\right), \tag{9}$$

$$G_{\mathrm{VRH}} = \frac{1}{2}\left(G_{\mathrm{V}} + G_{\mathrm{R}}\right), \tag{10}$$

$$E = \frac{9B_{\mathrm{VRH}}G_{\mathrm{VRH}}}{(3B_{\mathrm{VRH}} + G_{\mathrm{VRH}})}, \tag{11}$$

$$\sigma = \frac{(3B_{\mathrm{VRH}} - 2G_{\mathrm{VRH}})}{[2\,(3B_{\mathrm{VRH}} + G_{\mathrm{VRH}})]}. \tag{12}$$

The value of VRH refers to the average of the Reuss and Viogt, and the value of Reuss and the value of Viogt represent the maximum and minimum value of the elastic modulus, respectively (Eqs. (6)–(11)).[41,42] The calculated values of bulk modulus (B), shear modulus (G), Young's modulus (E), and Poisson's ratio (σ) of the Cr–Si compounds are shown in Table 4. To the best of our knowledge, the bulk modulus reflects the ability to compress a solid under hydrostatic pressure. All the Cr_xSi_y compounds each present a large bulk modulus. Therefore, they can potentially be superhard materials. The bulk modulus of the Cr_3Si compound with the lowest Si content is highest (251.0 GPa). The shear modulus and Young's modulus of $CrSi_2$ with the highest Si content are largest (169.5 GPa and 394.9 GPa, respectively). Generally speaking, the values of hardness and stiffness of the compounds are positively correlated with the value of shear modulus and Young's modulus. As shown in Table 3, the Poisson ratios of the Cr–Si system's values are calculated, which range from 0.164 to 0.239, illustrating that the covalent bonds in these structures are more directional. The results show that the brittle Cr–Si compounds have weak metal properties. The Poisson ratio greater or less than 0.25 indicates the toughness or brittleness of the compounds. The value of B/G is used to illustrate the brittleness and toughness of the compound.[43] The brittle behaves as the Cr–Si binary compound when the B/G ratio is less than the critical value of 1.75. Furthermore, Cr_3Si with the lowest Si content has the greatest B/G value of 1.59, while $CrSi_2$ with the highest Si atom content has the smallest B/G value of 1.16 of the Cr–B compound. The B/G value decreases with the increase of Si content, which indicates that the compounds exhibit more brittle behaviour.

In order to depict the mechanical properties of the Cr–B binary compounds, the elastic constant curves with the change of Si content are listed in Figs. 6 and 7. It can be seen that C_{44} and shear modulus (G) exhibit the same change trend, but the bulk modulus and C_{44} have no clear relationship. The Young modulus and (C_{11}–C_{12}) present a similar variation tendency as shown in Fig. 7.

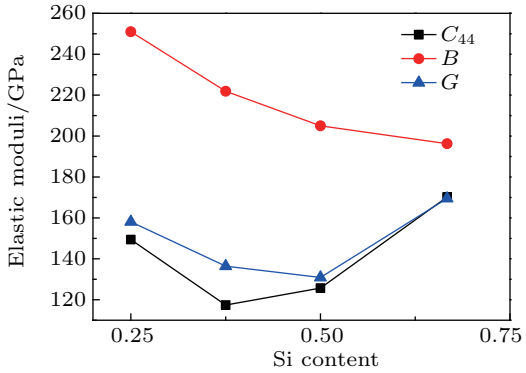


Fig. 6. (color online) Variations of bulk modulus, shear modulus, and C_{44} with Si content of Cr–B binary compounds.

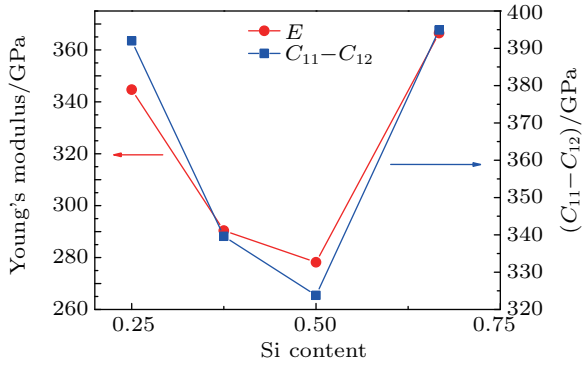


Fig. 7. (color online) Variations of (C_{11}–C_{12}) and Young's modulus with Si content of Cr–B binary compounds.

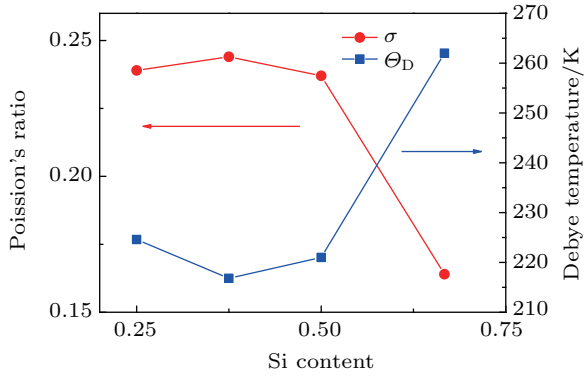


Fig. 8. (color online) Variations of Poisson's ratio and Debye temperature with Si content of Cr–B binary compounds.

3.4. Debye temperature

The specific heat, elastic constant, melting point, and chemical bonding properties of the compound can be reflected by the Debye temperature.[44] In this subsection, Debye temperature (HD) and average sound velocity (v_{m}) can be described by the following relations:[31,45,46]

$$\Theta_{\mathrm{D}} = \frac{h}{k_{\mathrm{B}}}\left[\frac{3n}{4\pi}\left(\frac{N_A\rho}{M}\right)\right]^{1/3} v_m, \tag{13}$$

$$v_{\mathrm{m}} = \left[\frac{1}{3}\left(\frac{2}{v_{\mathrm{s}}^3} + \frac{1}{v_{\mathrm{l}}^3}\right)\right]^{-(1/3)}, \tag{14}$$

$$v_{\rm l} = \sqrt{\frac{(B+(4/3)G)}{\rho}}, \tag{15}$$

$$v_{\rm s} = \sqrt{\frac{G}{\rho}}, \tag{16}$$

where $\Theta_{\rm D}$ is the Debye temperature; h and $k_{\rm B}$ are the Planck and Boltzmann constant, respectively; $N_{\rm A}$ and n are the Avogadro constant and the total number of atoms per formula, respectively; M represents the molecular weight per formula; $v_{\rm s}$, $v_{\rm l}$, and ρ are the transverse sound velocity, the longitudinal sound velocity, and the theoretical density, respectively; G is the shear modulus, and B represent the bulk modulus values.[47–49] The calculated results of sound velocity and Debye temperature for Cr–Si compounds are shown in Table 5. The Debye temperature can be reflected by the strength of covalent bond in the solid.[50] Table 5 shows that the $CrSi_2$ has the largest $\Theta_{\rm D}$ value (262.0 K) and Cr_5Si_3 has the lowest $\Theta_{\rm D}$ value (216.8 K). Therefore, it is concluded that the $CrSi_2$ has greater covalent bonds than other silicides and the Cr_5Si_3 has the strongest metallic character because of the highest B/G ratio and lowest $\Theta_{\rm D}$ value. In addition, as shown in Fig. 8, the $\Theta_{\rm D}$ value of silicides have an opposite trend to the Poisson ratio, which may be due to the fact that the compounds bonding features exhibit the effect trend of Poisson's ratio and Debye temperature. Moreover, the calculated average sound velocities of the compounds are larger, which are affected by their large elastic modulus and low density as well as the density, and the bulk modulus and shear modulus affect the v_1 and $v_{\rm s}$ values.

Table 5. Theoretical density (ρ in unit kg·m^{-3}), longitudinal sound velocity (v_1 in unit m·s^{-1}), transverse sound velocity ($v_{\rm s}$ in unit m·s^{-1}), average sound velocity (v_m in unit m·s^{-1}), and Debye temperature ($\Theta_{\rm D}$ in unit K).

Species	ρ	v_1	$v_{\rm s}$	$v_{\rm m}$	$\Theta_{\rm D}$
Cr_3Si	6648.59	8334.2	4876.4	5407.3	224.6
Cr_5Si_3	6061.15	8161.8	4743.9	5263.4	216.8
CrSi	5493.78	8311.5	4881.2	5410.7	221.0
$CrSi_2$	5051.70	9143.1	5792.5	6371.4	262.0

3.5. Mechanical anisotropy

The mechanical anisotropy is essential in the applications of Cr–Si materials. Micro cracks form not only on the surface, but also inside of the material. The formation and propagation of micro cracks relate to anisotropy. Cr–Si compounds act as one of the structural materials used in elevated temperature, and their mechanical anisotropy must be investigated. The following equations are combined to describe the degree of anisotropy, a number of parameters, including the anisotropic index (A_B and A_G), the shear anisotropic factors (A_1, A_2, and A_3) as well as universal anisotropic index ($A^{\rm U}$):[42,45]

$$A^{\rm U} = 5\frac{G_{\rm V}}{G_{\rm R}} + \frac{B_{\rm V}}{B_{\rm R}} - 6 \geq 0, \tag{17}$$

$$A_B = \frac{B_{\rm V} - B_{\rm R}}{B_{\rm V} + B_{\rm R}}, \tag{18}$$

$$A_G = \frac{G_{\rm V} - G_{\rm R}}{G_{\rm V} + G_{\rm R}}, \tag{19}$$

$$A_1 = \frac{4C_{44}}{G_{11} + C_{33} - 2C_{13}} \quad \text{for (100) plane}, \tag{20}$$

$$A_2 = \frac{4C_{55}}{G_{22} + C_{33} - 2C_{23}} \quad \text{for (010) plane}, \tag{21}$$

$$A_3 = \frac{4C_{66}}{G_{11} + C_{22} - 2C_{12}} \quad \text{for (001) plane}, \tag{22}$$

where $G_{\rm V}$ and $B_{\rm V}$ are the shear modulus and bulk modulus estimated by the Voigt method, and $G_{\rm R}$ and $B_{\rm R}$ are the shear modulus and bulk modulus estimated by the Reuss method, respectively. The unity value of shear anisotropy indicates the isotropic extent in the crystal. For example, B and G each have an approximate value, which expresses that the value of $A^{\rm U}$ is zero. The highly mechanical anisotropic properties are due to the greater anisotropy index ($A^{\rm U}$).

Table 6 shows that Cr_5Si_3 has the largest $A^{\rm U}$ value and Cr_3Si has the smallest AU value. The strong anisotropy is due to the fact that the value $A^{\rm U}$ is large. The universal anisotropic index ($A^{\rm U}$) can provide the corresponding results for the mechanical anisotropy. Therefore, the order of elastic anisotropy of Cr–Si compounds is as follows: Cr_5Si_3>$CrSi_2$>Cr_3Si>CrSi. Furthermore, the largest value of A_B is only 0.002% for all compounds, which implies that the bulk modulus anisotropy of a compound is weak. The shear modulus is more dependent on the direction which is confirmed by A_G, A_1, A_2, and A_3, but their functions are different. In different crystal planes, the values of A_1, A_2, and A_3 show the anisotropies of the shear modulus. The $CrSi_2$ (A_1 and A_2 value are both 1.11) has greater anisotropic indices of the shear modulus in the (100) and (010) plane respectively and the Cr_5Si_3 (A_3 value is 1.05) has the strongest anisotropic index of the shear modulus in the (001) plane.

Table 6. Calculated values of universal anisotropic index ($A^{\rm U}$), anisotropic indices (A_B and A_G), and shear anisotropic factors (A_1, A_2, and A_3) of Cr–Si compounds.

Species	$A^{\rm U}$	A_B/%	A_G	A_1	A_2	A_3
Cr_3Si	0.025	0	0.205(%)	0.87	0.87	0.87
Cr_5Si_3	0.084	0.002	0.81(%)	0.77	0.77	1.05
CrSi	0.015	0	0.15(%)	0.90	0.90	0.90
$CrSi_2$	0.044	0.001	0.41(%)	1.11	1.11	1.00

Young's modulus curved surface of three-dimensions (3D) would explain why the anisotropic properties are so much

simpler. The Young modulus is calculated on the basis of the following formulas:[51–53]

for the cubic crystal (for Cr_3Si, CrSi):

$$\frac{1}{E} = l_1^4 S_{11} + l_2^4 S_{22} + l_3^4 S_{33} + 2l_1^2 l_2^2 S_{12} + 2l_1^2 l_3^2 S_{13} + 2l_2^2 l_3^2 S_{23} + l_1^2 l_2^2 S_{66} + l_1^2 l_3^2 S_{55} + l_2^2 l_3^2 S_{44}; \quad (23)$$

for the tetragonal crystal (for Cr_5Si_3) and hexagonal crystal (for $CrSi_2$):

$$\frac{1}{E} = S_{11}(S_{11} - l_3^2)^2 + l_3^4 S_{33} + (2S_{13} + S_{44}) l_3^2 (1 - l_3^2), \quad (24)$$

where the S_{ij} values are the elastic compliance constants, and l_1, l_2, and l_3 are the directional cosines. The contour plots of the Young modulus of these Cr–Si compounds are illustrated in Fig. 9. We find that all the compounds show a strong anisotropic character in Young's modulus. According to the 3D curved surface and the color bar, we can see that the stronger the color, the greater the Young modulus is. However, the 3D curved surface of $CrSi_2$ is close to an ellipsoid that is different from others. It indicates that the Young modulus of $CrSi_2$ has weaker anisotropy than other compounds. Furthermore, plots of the Young modulus at different crystal planes of a crystal in more detail show the Cr–Si compounds' anisotropic properties as shown in Fig. 10. On the (100), (001), and (110) planes. The Young modulus is highly dependent on the direction. On the (100) plane direction, $CrSi_2$ exhibits the maximum value of Young's modulus in the [010] and [001] directions.

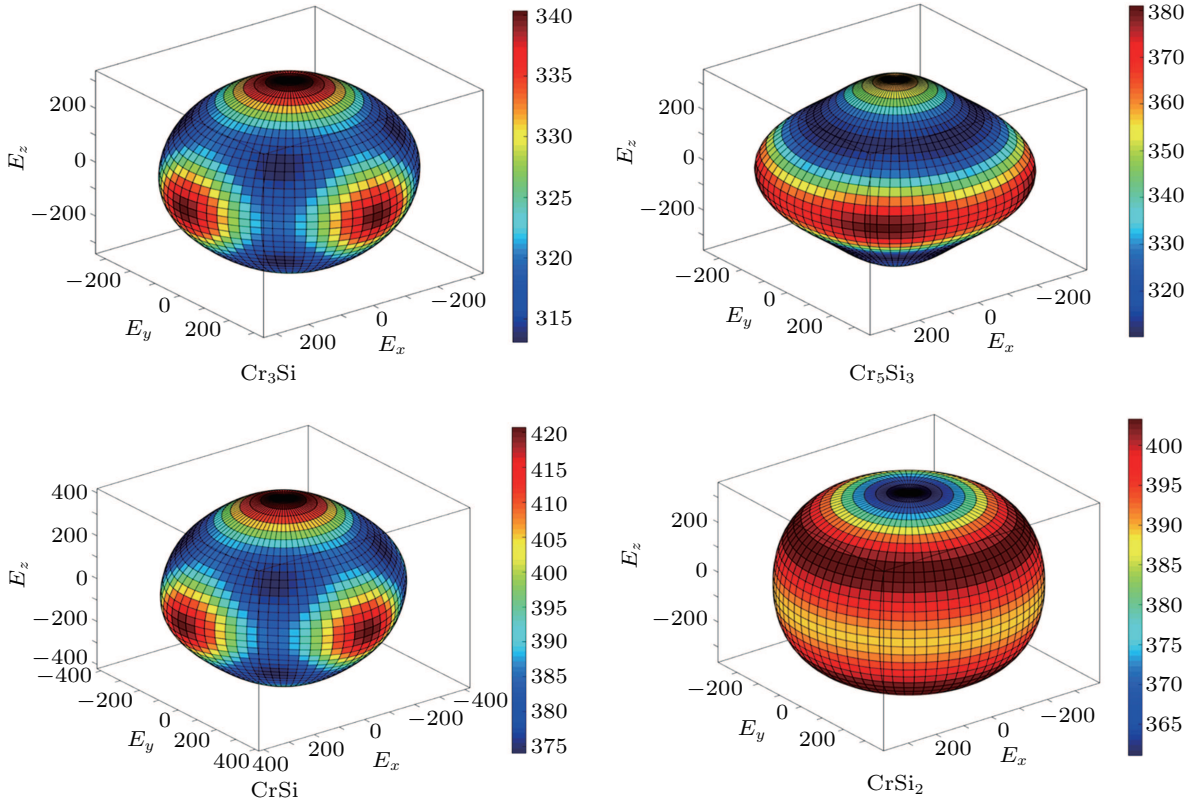


Fig. 9. (color online) Contour plots of Young's modulus of the Cr–Si compounds in 3-D space.

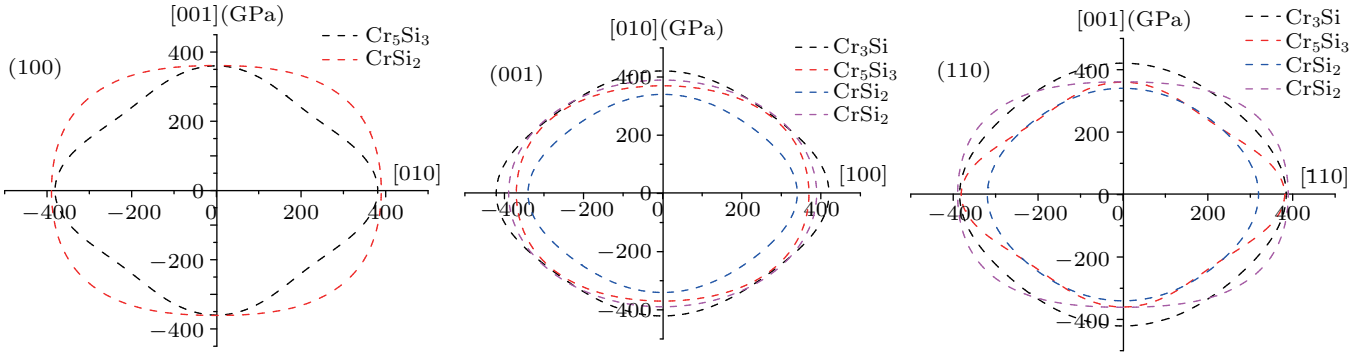


Fig. 10. (color online) Planar projections of Young's modulus of the Cr–Si compounds on (100), (001), and (110) crystallographic planes.

Moreover, in the [010] and [100] directions, the Cr_3Si exhibits the maximum value of Young's modulus, and Cr_5Si_3 shows the smallest Young's modulus on the (001) plane. In addition, the largest values of Young's modulus for Cr_5Si_3 and $CrSi_2$ deviate from their principal axes at the (110) plane. In addition, it is found that the CrSi shows the smallest Young's modulus in the [010] and [100] directions on the (001) plane. On the (001) and (110) planes, the planar contours of $CrSi_2$ seems to be a spherical shape, which means that the Young modulus of $CrSi_2$ has a weaker anisotropy than other compounds'.

4. Conclusions

The first-principle calculations, including the chemical stability, electronic structures, Debye temperature, and anisotropic properties are combined to investigate the properties of Cr–Si binary compounds. The calculated cohesive energy and formation enthalpy indicate the thermodynamical stability. From the electronic structures of the Cr–Si binary compounds, we deduce that the bonding characteristics are determined by Cr–Si covalent bonds, but also possess the metallic character. In particular, the $CrSi_2$ has stronger covalent bond properties than other silicides. The results show that the Cr_3Si has the highest value (251.0 GPa) of bulk modulus and the $CrSi_2$ has the highest values (169.5 GPa and 394.9 GPa) of shear modulus and Young's modulus, respectively. The value of Debye temperature indicates the strong covalent bonds of the Cr–Si compounds. The $CrSi_2$ has the largest Debye temperature (262.0 K), indicating stronger covalent bonds characters than others. To verify the mechanical anisotropy, the Young modulus of the Cr–Si binary compound is plotted by the 3D surface contour.

Acknowledgment

The authors thank those people for their scientific contributions to this work.

References

[1] Mattheiss L 1991 *Phys. Rev. B* **43** 12549
[2] Shah D, Berczik D, Anton D and Hecht R 1992 *Mater. Sci. Eng. A* **155** 45
[3] Qian-Gang F, He-Jun L, Xiao-Hong S, Xiao-Ling L, Ke-Zhi L and Min H 2006 *Appl. Surf. Sci.* **252** 3475
[4] Yeh C L and Lin J Z 2013 *Intermetallics* **33** 126
[5] Duan G and Wang H M 2002 *Scr. Mater.* **46** 107
[6] Okamoto H 2001 *J. Phase Equilibria* **22** 593
[7] Du Y and Schuster J C 2000 *J. Phase Equilibria* **21** 281
[8] Chen H, Du Y and Schuster J C 2009 *Calphad* **33** 211
[9] Krijn M and Eppenga R 1991 *Phys. Rev. B* **44** 9042
[10] Segall M D, Lindan P J D, Probert M J, Pickard C J, Hasnip P J, Clark S J and Payne M C 2002 *J. Phys.-Condes. Matter* **14** 2717
[11] Gao S, Xiang H, Xu B, Xia Y D , Yin J and Liu Z G 2016 *Chin. Phys. Lett.* **33** 083101
[12] Liu G, Liu S B, Xu B, Ouyang C Y and Song H Y 2015 *J. Appl. Phys.* **112** 666
[13] Gokhale A B and Abbaschian G J 1987 *J. Phase Equilibria* **8** 474
[14] Macdonald A H 1978 *Phys. Rev. B* **18** 5897
[15] Haiyang Z and Shunle D 2013 *Chin. Phys. Lett.* **30** 43102
[16] Pan L J, Zhang J, Chen W G and Tang Y N 2015 *Chin. Phys. Lett.* **32** 036101
[17] Cui S and Jung I H 2017 *J. Alloys Compd.* **708** 887
[18] Zhou S, Xie Q, Yan W and Chen Q 2009 *Sci. Chin.-Phys. Mech. Astron.* **52** 46
[19] Chart T G 2013 *Met. Sci.* **9** 504
[20] Jauch W, Schultz A J and Heger G 1987 *J. Appl. Crystallogr.* **20** 117
[21] Ma J, Gu Y, Shi L, Chen L, Yang Z and Qian Y 2004 *J. Alloys Compd.* **376** 176
[22] Meschel S V and Kleppa O J 1998 *J. Alloys Compd.* **267** 128
[23] Jurisch M and Behr G 1979 *Acta Phys. Acad. Sci. Hung.* **47** 201
[24] Coughanowr C A, Ansara I and Lukas H L 1994 *Calphad-Comput. Coupling Ph. Diagrams Thermochem.* **18** 125
[25] Dai Y Y, Li Y, Peng S M, Long X G, Fei G and Xiaotao Z U 2010 *Chin. Phys. Lett.* **27** 42
[26] Song Y J, Zhang Q H, Shen X, Ni X D, Yao Y and Yu R C 2014 *Chin. Phys. Lett.* **31** 017501
[27] Huang L T , Chen Z, Wang Y X and Lu Y L 2017 *Chin. Phys. B* **26** 103103
[28] Xie X D, Hao Y Y, Zhang R G and Wang B J 2012 *Acta Phys. Sin.* **61** 855 (in Chinese)
[29] Raheleh, Pilevar, Shahri, Arsalan and Akhtar 2017 *Chin. Phys. B* **26** 093107
[30] Chong X Y, Jiang Y H, Zhou R and Feng J 2014 *Comput. Mater. Sci.* **87** 19
[31] Feng J, Xiao B, Chen J, Du Y, Yu J and Zhou R 2011 *Mater.* **32** 3231
[32] Wen M and Wang C Y 2017 *Chin. Phys. B* **26** 093106
[33] Wu Z J, Zhao E J, Xiang H P, Hao X F, Liu X J and Meng J 2007 *Phys. Rev. B* 054115
[34] Patil S K R, Khare S V, Tuttle B R, Bording J K and Kodambaka S 2006 *Phys. Rev. B* **73** 4118
[35] Bei H, George E P and Pharr G M 2004 *Scr. Mater.* **51** 875
[36] Nakamura M 1994 *Metall. Mater. Trans. A* **25** 331
[37] Hermet P, Khalil M, Viennois R, Beaudhuin M, Bourgogne D and Ravot D 2015 *RSC Adv.* **5** 19106
[38] Zhang X, Wang Z and Qiao Y 2011 *Acta Mater.* **59** 5584
[39] Zhou W, Liu L, Li B, Wu P and Song Q 2009 *Comput. Mater. Sci.* **46** 921
[40] Zinoveva G P, Andreeva L P and Geld P V 1974 *Phys. Status Solidi* **23** 711
[41] Hill R W 1952 *Proc. Phys. Soc.* **65** 349
[42] Xiao B, Feng J, Zhou C T, Jiang Y H and Zhou R 2011 *J. RSC Adv.* **109** 083521
[43] Chong X, Jiang Y, Zhou R and Feng J 2014 *RSC Adv.* **4** 44959
[44] Wang J and Sun J 2010 *Phys. Status Solidi* **247** 921
[45] Feng J, Xiao B, Zhou R, Pan W and Clarke D R 2012 *Acta Mater.* **60** 3380
[46] Anderson O L 1963 *J. Phys. Chem. Solids* **24** 909
[47] Li Y, Gao Y, Xiao B, Min T, Fan Z, Ma S and Xu L 2010 *J. Alloys Compd.* **502** 28
[48] Liu Y Z, Jiang Y H, Zhou R and Feng J 2014 *J. Alloys Compd.* **582** 500
[49] Feng J, Xiao B, Wan C L, Qu Z X, Huang Z C, Chen J C, Zhou R and Pan W 2011 *Acta Mater.* **59** 1742
[50] Guechi A, Merabet A, Chegaar M, Bouhemadou A and Guechi N 2015 *J. Alloys Compd.* **623** 219
[51] Feng J, Xiao B, Zhou R and Pan W 2013 *Acta Mater.* **61** 7364
[52] Sun L, Gao Y, Xiao B, Li Y and Wang G 2013 *J. Alloys Compd.* **579** 457
[53] Panda K B and Chandran K S R 2006 *Acta Mater.* **54** 1641